Radiology

Micro–MR Imaging–based Computational Biomechanics Demonstrates Reduction in Cortical and Trabecular Bone Strength after Renal Transplantation[1]

Chamith S. Rajapakse, PhD
Mary B. Leonard, MD, MSCE
Yusuf A. Bhagat, PhD
Wenli Sun, MS
Jeremy F. Magland, PhD
Felix W. Wehrli, PhD

Purpose: To examine the ability of three-dimensional micro–magnetic resonance (MR) imaging–based computational biomechanics to detect mechanical alterations in trabecular bone and cortical bone in the distal tibia of incident renal transplant recipients 6 months after renal transplantation and compare them with bone mineral density (BMD) outcomes.

Materials and Methods: The study was approved by the institutional review board and complied with HIPAA guidelines. Written informed consent was obtained from all subjects. Micro–MR imaging of distal tibial metaphysis was performed within 2 weeks after renal transplantation (baseline) and 6 months later in 49 participants (24 female; median age, 44 years; range, 19–61 years) with a clinical 1.5-T whole-body imager using a modified three-dimensional fast large-angle spin-echo pulse sequence. Micro–finite-element models for cortical bone, trabecular bone, and whole-bone section were generated from each image by delineating the endosteal and periosteal boundaries. Mechanical parameters (stiffness and failure load) were estimated with simulated uniaxial compression tests on the micro–finite-element models. Structural parameters (trabecular bone volume fraction [BV/TV, bone volume to total volume ratio], trabecular thickness [TbTh], and cortical thickness [CtTh]) were computed from micro-MR images. Total hip and spine areal BMD were determined with dual-energy x-ray absorptiometry (DXA). Parameters obtained at the follow-up were compared with the baseline values by using parametric or nonparametric tests depending on the normality of data.

Results: All mechanical parameters were significantly lower at 6 months compared with baseline. Decreases in cortical bone, trabecular bone, and whole-bone stiffness were 3.7% ($P = .03$), 4.9% ($P = .03$), and 4.3% ($P = .003$), respectively. Decreases in cortical bone, trabecular bone, and whole-bone failure strength were 7.6% ($P = .0003$), 6.0% ($P = .004$), and 5.6% ($P = .0004$), respectively. Conventional structural measures, BV/TV, TbTh, and CtTh, did not change significantly. Spine BMD decreased by 2.9% ($P < .0001$), while hip BMD did not change significantly at DXA.

Conclusion: MR imaging–based micro–finite-element analysis suggests that stiffness and failure strength of the distal tibia decrease over a 6-month interval after renal transplantation.

©RSNA, 2012

Renal osteodystrophy is a multifactorial disorder of bone metabolism that occurs in patients with end-stage renal disease (1). As renal failure progresses, abnormal parathyroid hormone secretion results in increased bone-volume fraction (BVF [BV/TV, bone volume to total volume ratio]), abnormal trabecular connectivity, cortical thinning, and decreased cortical bone mineral density (BMD) (2,3). Despite widespread use of phosphate binders and vitamin D therapies, bone fracture rates in young adults undergoing dialysis are increased 100-fold (4). Successful renal transplantation corrects many of the underlying abnormalities contributing to renal osteodystrophy (5). However, persistent hyperparathyroidism and immunosuppressive therapies may lead to further bone loss (6). The risk of fracture among renal transplant recipients increases even further in the months following surgery (7). Interestingly, post-transplantation bone fractures are more frequently located in the appendicular than axial skeleton (8–10).

Dual-energy x-ray absorptiometry (DXA) does not allow distinction between the effect of renal osteodystrophy on cortical and trabecular bone and provides poor fracture discrimination in patients with renal failure (8,11). Consequently, international guidelines recommend that DXA BMD testing not be performed routinely in renal transplant recipients (12). In contrast, quantitative computed tomography (CT) measures of appendicular cortical BMD and cortical thickness (CtTh) provide greater fracture discrimination (11). The only previously published quantitative CT study in adult renal transplant recipients was cross-sectional and was conducted in 12 patients 1–58 months

after transplantation; it demonstrated significant cortical thinning (13).

Micro–magnetic resonance (MR) imaging (14,15) and high-resolution peripheral quantitative CT (16,17) now permit in-vivo noninvasive acquisition of images at peripheral locations at resolutions adequate to resolve three-dimensional (3D) microarchitecture of the bone. Since micro–MR imaging does not involve ionizing radiation, it is particularly suited for repeated short-term evaluation of bone disease in the immediate post-transplantation period. In a cross-sectional study, Link et al (18) reported significant differences in structural measures of trabecular bone in renal transplant recipients and of the calcaneus in control subjects.

BMD and bone structural parameters are surrogates for bone strength and fracture susceptibility. Micro-finite-element analysis provides a more direct assessment of the mechanical competence of bone (19). A recent study demonstrated that in vivo micro–MR imaging generates accurate 3D models of bone that serve as input into the micro-finite-element simulator (20), yielding biomechanical measures of bone strength in response to intervention (21,22).

Cortical and trabecular bone compartments are known to get affected differently in transplant recipients depending on various causes and forms of post-transplantation bone disease. Perturbation in cortical bone, for example, is more pronounced in patients with persistent secondary hyperparathyroidism following transplantation (23,24) and is manifested as cortical bone thinning, intracortical resorption, and trabecularization of the endosteal cortex (3,25). Trabecular bone, on the other hand, is more susceptible to the effects of glucocorticosteroids (26,27),

especially during the initial months following the transplantation when doses are generally high enough to directly suppress bone formation. These structural deteriorations of cortical and trabecular bone could persist even without detectable abnormalities in serum calcium, phosphorus, or vitamin D levels (3). A method sensitive to mechanical alterations in both cortical and trabecular bone, therefore, could improve our understanding of the spectrum of post-transplantation bone disease.

The purpose of this study was to examine the ability of 3D micro–MR imaging–based computational biomechanics to detect mechanical alterations in cortical and trabecular bone in the distal tibia of incident renal transplant recipients 6 months after transplantation and compare them with BMD outcomes.

Materials and Methods

Study Subjects

This prospective study consisted of 24 female (10 postmenopausal; mean age,

Advance in Knowledge

- In-vivo MR imaging–based micro–finite-element analysis suggests that stiffness and failure strength of distal tibia are reduced during a 6-month interval after renal transplantation.

Implication for Patient Care

- Micro–MR imaging–based micro–finite-element analysis has potential for estimating short-term alterations in bone stiffness and failure strength in renal transplant recipients.

38 years; range, 19–51 years) and 25 male (mean age, 45 years; range, 25–61 years) renal transplant recipients at transplantation at a single transplant center examined between April 2008 and April 2011. Only 32 subjects were undergoing dialysis prior to transplantation for a median of 2.4 years (range, 0.1–6.2 years). The primary cause of renal disease in the cohort was heterogeneous: hereditary or congenital cystic diseases ($n = 11$), glomerulonephritis ($n = 11$), focal segmental glomerulosclerosis ($n = 10$), hypertensive disease ($n = 7$), type I diabetes ($n = 3$), type II diabetes ($n = 3$), and etiology uncertain ($n = 4$). Plasma intact parathyroid hormone levels, quantified by using radioimmunoassay with iodine 125–labeled antibody (Scantibodies Clinical Laboratory, Santee, Calif), were 25–479 pg/mL (median, 149 pg/mL) at renal transplantation. Twenty-one subjects had a history of fractures (four of low impact). Exclusion criteria included prior organ transplantation, simultaneous pancreas transplantation, prior lower extremity amputation or difficulty with ambulation, systemic inflammatory disease, or glucocorticoid therapy within 6 months prior to renal transplantation. All allograft recipients were treated with an immunosuppressive regimen that included glucocorticoids and were also receiving various other medications for various medical conditions. The study was approved by the authors' institutional review board and complied with Health Insurance Portability and Accountability Act guidelines. Written informed consent was obtained from all subjects.

Image Acquisition

Micro-MR and DXA images were obtained within 2 weeks (baseline) and 6 months $\pm$ 0.5 (standard deviation) after renal transplantation. Lumbar spine (L1–L4) and total hip BMD were assessed at DXA with a bone densitometer (QDR 4500; Hologic, Bedford, Mass) in the array mode by using standard positioning techniques. MR images were obtained with a commercial 1.5-T whole-body imager (Siemens Sonata, Erlangen, Germany), with the
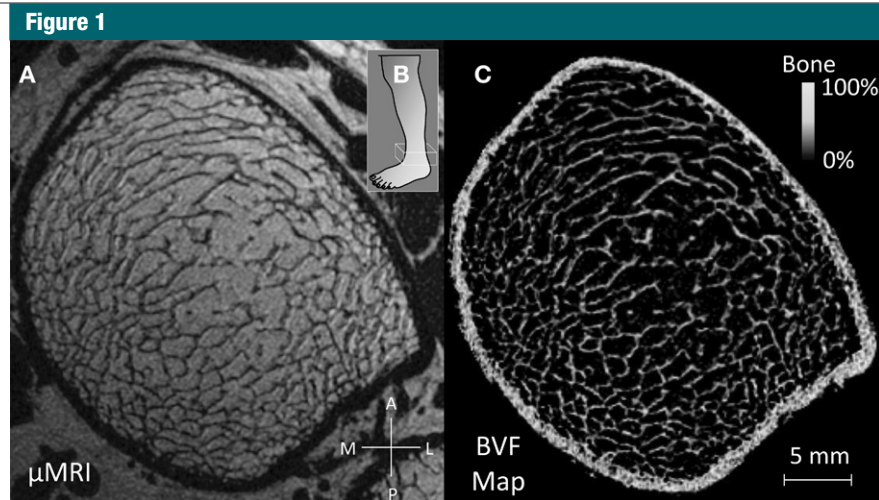
Figure 1

Figure 1: *A,* Midaxial 3D FLASE micro-MR image obtained at left distal tibial metaphysis (*B,* inset) in 25-year-old woman. *C,* Corresponding BVF map represents fractional occupancy of bone linearly scaled between 0% (pure marrow) and 100% (pure bone) at each voxel. *A-P* = anteroposterior axis, , *M-L* = mediolateral axis.

subjects in feet-first supine position. A custom-designed two-element receive-only surface coil was placed anteriorly on the left ankle (right ankle if the left ankle had a previous fracture) so that the coil was about 1 cm proximal to the midpoint of the medial malleolus. The entire foot was immobilized by using a vacuum bag (VacFix; Soule Medical Systems, Lutz, Fla), and hook-and-loop fasteners were placed around the lower foot and the coil. Preparatory pulse sequences included two two-dimensional gradient-echo localizers to ensure correct coil positioning relative to the tibial end-plate, two spin-echo sequences (one axial, one sagittal) to aid in the placement of the high-resolution imaging volume, and a 3D fast gradient-echo sequence for prospective registration (28) between baseline and follow-up acquisitions. Subsequently, MR acquisitions were performed at tibial metaphysis covering a $70 \times 64 \times 13$ mm^3 volume (with the third dimension being along the axial direction) centered 16.5 mm proximal to the distal end-plate of the tibia by using a modified fast large-angle spin-echo, or FLASE, pulse sequence (29). Three-dimensional FLASE images were acquired (Fig 1) with a 140° flip angle, repetition time msec/echo time msec of 80/11.8 (60% fractional-echo acquisition), 16.67-kHz

bandwidth, and $137 \times 137 \times 410$ μm^3 voxel size in 15 minutes 23 seconds.

Image Processing

The raw micro-MR data were corrected for involuntary subject motion during imaging by using the navigator data obtained during the FLASE acquisition (30) and by autofocusing (31). The image with the best overall quality out of the three images (non–motion-corrected, navigator, and autofocus) was selected for further processing by agreement of four blinded raters (32). Image intensity variations across the imaging volume caused by inhomogeneous sensitivity of the MR imaging receiver coil were corrected by using local a thresholding algorithm (33). Subsequently, coregistered transaxial slabs of 8 mm thickness were extracted from the 3D FLASE dataset at the two time points for each subject (34). The gray-scale values of the images were linearly scaled to cover the range from 0% to 100%, with pure marrow and pure bone having minimum and maximum values, respectively. We refer to the resulting 3D array as the BVF map, with individual voxel values representing the fraction of the voxel occupied by bone (Fig 1). Finally, three sets of 3D volumes, referred to as cortical compartment, trabecular compartment,

and whole section, were extracted from each image by delineating the endosteal and periosteal boundaries with use of a custom-designed operator-guided segmentation algorithm (Fig 2) (35).

Micro–Finite-Element Model Generation

To create a micro–finite-element model, each voxel in the BVF map was represented as a hexahedral finite element with dimensions equal to the voxel size. Bone was assumed to be composed of an empirically determined tissue modulus of 15 GPa and Poisson ratio of 0.3 (36). The tissue moduli of all models at each finite element were linearly scaled by the BVF value of the corresponding voxel to account for partial volume effects in the limited spatial resolution regimen of in vivo micro–MR imaging. In this manner, three sets of micro-finite-element models corresponding to the cortical compartment, trabecular compartment, and whole section were generated for each subject at each time point.

Computation of Stiffness

To estimate axial stiffness of the cortical compartment, trabecular compartment, and whole section, compressive loading was simulated in the linear elastic regimen. Here, 1% axial strain was applied to the proximal face of the micro-finite-element model while the distal face was kept constrained in the axial direction and frictionless conditions along the transverse directions were assumed (Fig 3). The nodes on the lateral sides were not constrained, allowing three degrees of freedom. The micro-finite-element models were then solved by minimizing the total strain energy resulting in equilibrium displacements at each finite element node. Axial stiffness was obtained as the ratio of the stress on the proximal face to the applied strain.

Computation of Failure Strength

To estimate the failure strength of the cortical compartment, trabecular compartment, and whole section of the tibia, it was assumed that the bone would fail when a substantial portion of bone (2% in this study) was strained beyond a critical limit, known as the tissue yield strain, following an approach

Figure 2
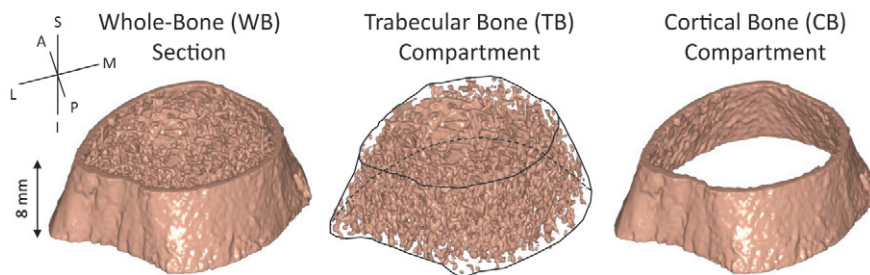
Figure 2: Micro-MR–derived 3D rendition of distal tibial metaphysis in 25-year-old female renal transplant recipient before and after isolation of trabecular and cortical bone compartments for subsequent micro-finite-element analysis. *A-P, M-L,* and *I-S* are anteroposterior, mediolateral, and inferosuperior axes, respectively.

Figure 3
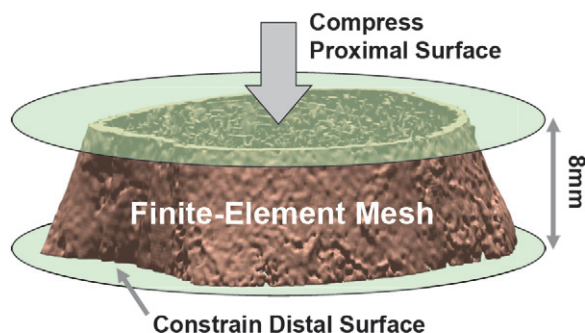
Figure 3: Illustration of simulated compression test on whole-bone section of distal tibia. The proximal surface is subjected to 1% strain along the inferosuperior axis, while the distal surface is constrained in the loading direction.

established by Pistoia et al (37). Bone tissue yield strain was chosen to be 0.007 (0.7%), as reported in the literature (38,39).

Structural and DXA Measures

Trabecular volume (BV/TV, bone volume to total volume ratio) was derived from the 3D BVF map as the mean fractional occupancy of bone over all voxels within the trabecular compartment (33). Trabecular thickness (TbTh) was computed by using the fuzzy-distance transform (40). Mean CtTh was calculated by modeling the endosteal and periosteal boundaries on each axial imaging section as concentric circles whose radii were estimated from the respective encompassed areas. Total hip and spine areal BMD were determined at DXA.

Statistical Analysis

The changes in parameters between baseline and follow-up time points were assessed by using two-sided paired Student *t* tests when data were normally distributed and nonparametric Wilcoxon signed rank test when data were not normally distributed. Correlations between failure strengths and other parameters were evaluated in terms of the Pearson correlation when data were normally distributed and Spearman correlation when data were not normally distributed. Results are reported as means ± standard deviations. All statistical analyses were performed by using software (JMP Discovery, version 7.0; SAS Institute, Cary, NC). A *P* value < .05 indicated a statistically significant difference.

Results

Mechanical Measures

Baseline and follow-up *P* values of micro-finite-element–derived distal tibial stiffness and failure strength and their observed changes between the

two time points are listed in Table 1. Axial stiffness and failure strength for cortical compartment, trabecular compartment, and whole section decreased significantly between the two time points, with failure strength showing the greatest temporal change among all the parameters computed. Overall, mechanical competence of the distal tibial metaphysis deteriorated substantially after renal transplantation, resulting from various mechanisms of bone loss, such as thinning of trabecular rods and perforations of trabecular plates (Fig 4).

Structural Measures

Three surrogate structural measures of bone quality commonly used in translational studies—trabecular volume (BV/TV), TbTh, and CtTh—did not show any significant change at 6 months compared with the baseline values (Table 2).

DXA Results

BMD measured at two central skeletal sites (routine clinical standard) showed inconsistent results for the temporal change (Table 2). While the decrease in spine BMD for the cohort was highly significant, albeit small (<3%, $P <$ .0001), BMD at the hip did not change between the two time points.

Associations of Parameters with Failure Strength

Baseline values of failure strength were weakly or moderately correlated (R^2 = 0.12–0.52) with several parameters computed from the same region of the tibia (Table 3). Failure strengths were only weakly correlated with hip BMD (R^2 = 0.14–0.25), while showing no correlation with spine BMD.

Associations among Temporal Changes in Parameters

Unlike absolute values, the percentage decrease in failure strength of cortical compartment, trabecular compartment, and whole section within the first 6 months of transplantation was highly correlated with that for axial stiffness values (R^2 = 0.80, 0.89, and 0.83, respectively; Table 4). Changes in BV/TV were moderately correlated with those in trabecular compartment

Table 1

Micro–Finite-Element–derived Mechanical Parameters (*n* = 49)

| Parameter	Baseline*	6 Months*	Percentage Change†	P Value‡
Cortical bone compartment				
Stiffness (MPa)	469 ± 135	447 ± 126	−3.72 (−12.45 to 5.23)	.03
Failure strength (kN)	2.33 ± 0.61	2.13 ± 0.57	−7.61 (−16.88 to 2.24)	.0003
Trabecular bone compartment				
Stiffness (MPa)	728 ± 162	699 ± 191	−4.94 (−11.78 to 3.73)	.03
Failure strength (kN)	3.25 ± 1.01	3.06 ± 1.04	−5.95 (−11.87 to 2.85)	.004
Whole-bone section				
Stiffness (MPa)	1328 ± 236	1275 ± 268	−4.29 (−10.31 to 3.53)	.003
Failure strength (kN)	5.77 ± 1.36	5.44 ± 1.40	−5.61 (−14.23 to 1.50)	.0004

Notes.—Whole-bone parameters were normally distributed, while cortical bone and trabecular bone parameters were not.

* Data are means ± standard deviations.

† Data are means and data in parentheses are interquartile range.

‡ *P* values correspond to absolute differences (paired *t* test or Wilcoxon test).

Figure 4
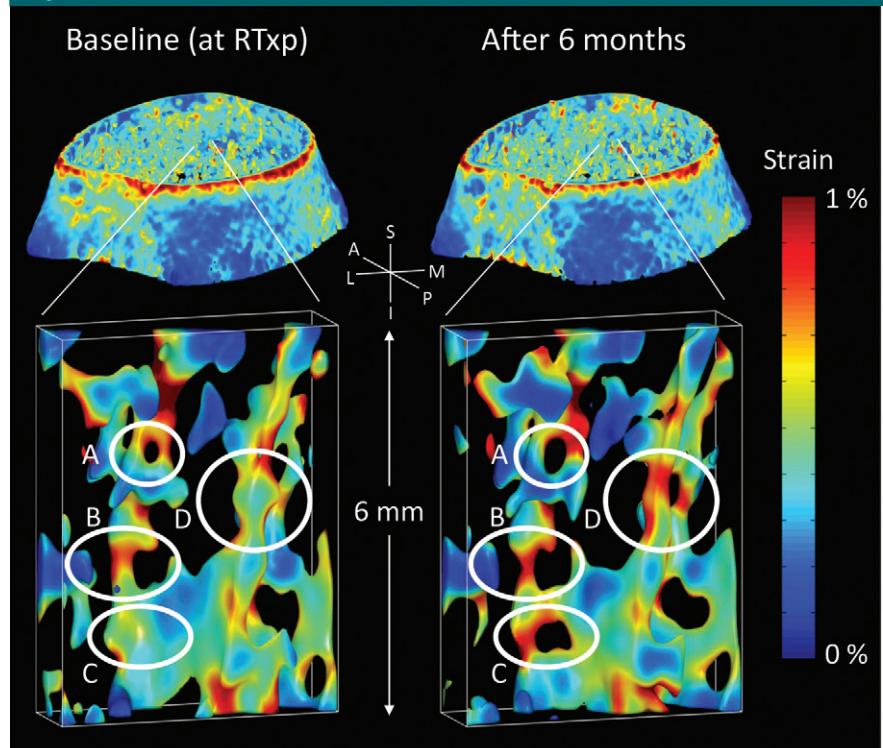
Figure 4: Comparison of strain maps obtained from whole-bone section micro-finite-element analysis in 25-year-old woman at baseline and 6 months after renal transplantation *(RTxp)*. The magnified 1 mm × 2 mm × 6 mm regions highlight various alterations taking place in the trabecular bone network between the two time points. *A* = enlargement of a perforation, *B* = thinning of vertical trabecula, *C* = a plate-to-rod conversion, and *D* = strain accumulation due to bone loss. *A-P, M-L,* and *I-S* are anteroposterior, mediolateral, and inferosuperior axes, respectively.

and whole-section failure strength (R^2 = 0.37 and 0.47) but not with cortical compartment failure strength. Interestingly, the percentage change in spine or hip BMD did not show any correlation with that in failure strengths.

Table 2

Micro-MR–derived Structural Parameters at Distal Tibia and DXA-derived BMD Measures at Spine and Hip (n = 49)

Parameter	Baseline*	6 Months*	Percentage Change†	P Value‡
Distal tibia				
BV/TV (%)	10.0 ± 1.3	10.0 ± 1.2	1.11 (−4.84 to 6.21)	.6
TbTh (μm)	109 ± 5.8	109 ± 5.1	−0.45 (−1.42 to 0.67)	.3
CtTh (μm)	1512 ± 153	1489 ± 172	−1.36 (−6.14 to 5.21)	.2
Total Spine BMD (mg/cm²)	1039 ± 155	1016 ± 155	−2.89 (−5.83 to −0.15)	<.0001
Total Hip BMD (mg/cm²)	912 ± 152	911 ± 156	0.60 (−3.07 to 2.06)	.9

Note.—All parameters except TbTh were normally distributed.

* Data are means ± standard deviations.

† Data are means and numbers in parentheses are interquartile range.

‡ P values correspond to absolute differences (paired t test or Wilcoxon test).

Table 3

Correlation between Failure Strength and Other Mechanical, Structural, and BMD Measures (n = 49) in Distal Tibia

Parameter	Cortical Bone Failure Strength		Trabecular Bone Failure Strength		Whole-Bone Failure Strength	
	R^2	P Value	R^2	P Value	R^2	P Value
Cortical bone stiffness	0.45	<.0001	0.05	.1	0.01	.5
Trabecular bone stiffness	0.0001	.9	0.52	<.0001	0.31	<.0001
Whole-bone stiffness	0.10	.02	0.14	.009	0.19	.002
BV/TV	0.05	.1	0.30	<.0001	0.32	<.0001
TbTh	0.01	.5	0.08	.04	0.09	.04
CtTh	0.30	<.0001	0.02	.4	0.12	.02
Spine BMD	0.08	.06	0.03	.3	0.06	.1
Hip BMD	0.21	.001	0.14	.009	0.25	.0004

Table 4

Correlation between Percentage Change in Failure Strength and Other Mechanical, Structural, and BMD Measures in Distal Tibia during First 6 Months after Renal Transplantation (n = 49)

Parameter	Cortical Bone Failure Strength		Trabecular Bone Failure Strength		Whole-Bone Failure Strength	
	R^2	P Value	R^2	P Value	R^2	P Value
Cortical bone stiffness	0.80	<.0001	0.01	.5	0.25	.0002
Trabecular bone stiffness	0.002	.8	0.89	<.0001	0.56	<.0001
Whole-bone stiffness	0.15	.006	0.74	<.0001	0.83	<.0001
BV/TV	0.05	.1	0.37	<.0001	0.47	<.0001
TbTh	0.03	.2	0.15	.006	0.20	.001
CtTh	0.03	.2	0.003	.7	0.04	.2
Spine BMD	0.00002	.98	0.02	.4	0.01	.5
Hip BMD	0.008	.6	0.001	.8	0.002	.8

Discussion

The changes in skeletal mechanical competence following renal transplantation are not well understood. The majority of studies relied on DXA (8,9,23,26,41–46); work based on advanced imaging techniques is limited to cross-sectional studies conducted at highly variable time points after transplantation (13,18). For example, there is a disconnect between fracture susceptibility and BMD, which has been ascribed to adverse effects of the disease on bone quality (3,8,9) and differences in the 3D microarchitecture of the bone between allograft recipients relative to their otherwise healthy peers with similar BMD (47). In this longitudinal study, we investigated the short-term effects on mechanical properties of bone— stiffness and failure strength—in renal transplant recipients on the basis of micro-finite-element models generated from micro-MR images of distal tibial metaphysis.

The present data indicate that mechanical competence of bone, measured in terms of stiffness and failure strength of cortical and trabecular compartments, deteriorates at least during the initial 6 months after renal transplantation. The mechanical weakening of cortical bone could be due to persistent secondary hyperparathyroidism, manifested as cortical thinning, intracortical resorption, and trabecularization of the endosteal cortex (23,24). Trabecular bone, on the other hand, is more susceptible to the effects of corticosteroids (3,25), especially during the initial months following transplantation, when doses are generally high enough to directly suppress bone formation.

In the current study, renal transplant recipients showed a decrease in stiffness and failure strength during the first 6 months following transplantation, while BV/TV did not change substantially. During the same period, spine BMD decreased, while hip BMD did not. In accordance, a number of prior studies confirmed that BV/TV is not altered on the basis of trans-iliac histomorphometry, and spine BMD decreases only slightly during the first

6 months after transplantation despite a substantial increase in fracture incidence (26,48,49). Furthermore, the data indicate that the trabecular compartment has greater stiffness and failure strength at baseline than does the cortical compartment due to the thin and generally trabeculated cortical bone at the distal tibia as opposed to the shafts of long bones, where bone is predominantly cortical. This observation is in agreement with that of McNeil et al, who reported that the mean load carried by the trabecular compartment at the distal tibia was around 71% of the total load based on measurements performed in 11 human subjects (age, 20–57 years) with high-resolution peripheral quantitative CT (50).

Micro–MR imaging acquisition and processing techniques detailed in this work provide a means for capturing short-term microstructural and mechanical disturbances of bone in vivo. Recent data show that mechanical parameters derived from micro–MR imaging–based micro–finite-element analysis at resolutions achievable in vivo correlate well with those obtained by means of the reference standard, thin-section micro-CT (20,51).

Although the usefulness of nonlinear micro–finite-element analysis in predicting bone strength has been demonstrated by using highly parallel supercomputers (52), computations in the present work were confined to the linear-elastic regimen so that the mechanical analysis could be performed by using high-end desktop computer systems within a clinically practical computation time. Nevertheless, mechanical parameters computed in the linear regimen have been shown to be highly correlated to yield strength with use of laboratory mechanical testing of specimens (19). Thus, linear micro-finite-element analysis provides a practical approach to compare relative bone strength and indirectly obtain information on the behavior of bone in the nonlinear regimen via Pistoia criterion (37). Of note is that the temporal changes in stiffness values found were highly predictive of those for failure strength.

Further, the data highlight that temporal changes in BMD measured at the hip and spine are not associated with detected alterations in stiffness and failure strength at the appendicular sites, which are particularly prone to fracture in renal transplant recipients (6,8–10). Additionally, baseline values of failure strength were only weakly correlated with hip BMD while showing no correlation with spine BMD. These observations are in agreement with data reported by Grotz et al (9), who found DXA BMD at the femoral neck and lumbar spine to be of limited or no value in identifying renal transplant recipients at risk for fracture.

Last, the data in this work suggest that short-term structural alterations and their mechanical implications in terms of local strain concentration are detectable in individual patients, which was not previously possible in vivo. Recent technologic advances in subject motion correction (30,31) and serial image registration (28,34) have improved our ability to detect structural changes in response to intervention by enhancing the reproducibility of MR imaging–based mechanical measures (53,54).

The study had limitations. First, the mechanical assessment was confined to a peripheral skeletal site (tibial metaphysis) since high-spatial-resolution micro-MR imaging of the hip is still in its infancy (55) and radiation dose exposure all but precludes thin-section CT imaging of central locations. Nevertheless, prior work has shown structural measures at peripheral sites to be predictive of vertebral fractures (56,57). Therefore, short-term mechanical degradation observed in renal transplant recipients at the distal tibia may also reflect such alterations at other skeletal sites, given the systemic nature of bone loss. However, further investigations are needed to evaluate the relationship between micro–finite-element–derived mechanical measures of cortical and trabecular bone at peripheral sites and mechanical competence of the hip and spine. Second, the loading conditions used for micro–finite-element analysis (ie, axial compression) do not

necessarily simulate physiologic boundary conditions during a fall that results in fracture. However, the strength of long bones under axial compression is predictive of that under bending and loading configurations that occur during a fall (58). Third, the assumed tissue modulus (15 GPa) and Poisson ratio of 0.3 may not reflect the true values for individual subjects because these physical parameters can be dependent on the subject and anatomic site (36). However, since each patient is his/her own control, the relative temporal changes in stiffness and failure load reported here are invariant to the true tissue modulus. Fourth, long-term effects of renal transplantation on bone cannot be inferred on the basis of data obtained from this relatively short-term study. Successful restoration of renal function could eventually reverse the mechanical disturbances observed in this study. Fifth, the study population was heterogeneous in terms of age and prior dialysis history. Nevertheless, patients with substantial comorbidities, prior transplantation, recent glucocorticoid therapy, and systemic inflammatory disease were excluded to minimize heterogeneity, and all subjects had been treated with an immunosuppressive regimen.

In summary, the work presented shows that micro–MR imaging of cortical and trabecular bone, in conjunction with micro–finite-element modeling, can provide insight into the short-term structural and mechanical manifestations of renal transplantation. An important strength of this study is the assessment of patients at the time of transplantation and again 6 months later—allowing distinction between the impact of the underlying end-stage renal disease and changes following renal transplantation. Further work in larger cohorts of patients and over-extended post-transplantation periods will be needed to corroborate the mechanical effects of the intervention and their relationship to fracture susceptibility. Importantly, future studies will evaluate the fracture discrimination and diagnostic test characteristics, compared with DXA.

Radiology

References

1. Hruska KA, Teitelbaum SL. Renal osteodystrophy. N Engl J Med 1995;333(3):166–174.

2. Amling M, Grote HJ, Vogel M, Hahn M, Delling G. Three-dimensional analysis of the spine in autopsy cases with renal osteodystrophy. Kidney Int 1994;46(3):733–743.

3. Parfitt AM. A structural approach to renal bone disease. J Bone Miner Res 1998;13(8):1213–1220.

4. Alem AM, Sherrard DJ, Gillen DL, et al. Increased risk of hip fracture among patients with end-stage renal disease. Kidney Int 2000;58(1):396–399.

5. Hariharan S, McBride MA, Cherikh WS, Tolleris CB, Bresnahan BA, Johnson CP. Post-transplant renal function in the first year predicts long-term kidney transplant survival. Kidney Int 2002;62(1):311–318.

6. Bia M. Evaluation and management of bone disease and fractures post transplant. Transplant Rev (Orlando) 2008;22(1):52–61.

7. Ball AM, Gillen DL, Sherrard D, et al. Risk of hip fracture among dialysis and renal transplant recipients. JAMA 2002;288(23):3014–3018.

8. Durieux S, Mercadal L, Orcel P, et al. Bone mineral density and fracture prevalence in long-term kidney graft recipients. Transplantation 2002;74(4):496–500.

9. Grotz WH, Mundinger FA, Gugel B, Exner V, Kirste G, Schollmeyer PJ. Bone fracture and osteodensitometry with dual energy x-ray absorptiometry in kidney transplant recipients. Transplantation 1994;58(8):912–915.

10. Ramsey-Goldman R, Dunn JE, Dunlop DD, et al. Increased risk of fracture in patients receiving solid organ transplants. J Bone Miner Res 1999;14(3):456–463.

11. Jamal SA, Gilbert J, Gordon C, Bauer DC. Cortical pQCT measures are associated with fractures in dialysis patients. J Bone Miner Res 2006;21(4):543–548.

12. Kidney Disease: Improving Global Outcomes (KDIGO) CKD-MBD Work Group. KDIGO clinical practice guideline for the diagnosis, evaluation, prevention, and treatment of chronic kidney disease-mineral and bone disorder (CKD-MBD). Kidney Int Suppl 2009;(113):S1–S130.

13. Negri AL, Lombas C, Cuevas C, Schiavelli R, Bogado CE, Zanchetta JR. Evaluation of cortical bone by peripheral quantitative computed tomography in renal transplant recipients. Transplant Proc 2005;37(2):1020–1022.

14. Krug R, Han ET, Banerjee S, Majumdar S. Fully balanced steady-state 3D-spin-echo (bSSSE) imaging at 3 Tesla. Magn Reson Med 2006;56(5):1033–1040.

15. Magland JF, Rajapakse CS, Wright AC, Acciavatti R, Wehrli FW. 3D fast spin echo with out-of-slab cancellation: a technique for high-resolution structural imaging of trabecular bone at 7 Tesla. Magn Reson Med 2010;63(3):719–727.

16. Boutroy S, Bouxsein ML, Munoz F, Delmas PD. In vivo assessment of trabecular bone microarchitecture by high-resolution peripheral quantitative computed tomography. J Clin Endocrinol Metab 2005;90(12):6508–6515.

17. Laib A, Hammerle S, Koller B. A new 100 µm resolution scanner for in vivo 3D-CT of the human forearm and lower leg. Presented at the 16th International Bone Densitometry Workshop, Annecy, France, June 20–24, 2004.

18. Link TM, Saborowski, Kisters K, et al. Changes in calcaneal trabecular bone structure assessed with high-resolution MR imaging in patients with kidney transplantation. Osteoporos Int 2002;13(2):119–129.

19. Macneil JA, Boyd SK. Bone strength at the distal radius can be estimated from high-resolution peripheral quantitative computed tomography and the finite element method. Bone 2008;42(6):1203–1213.

20. Rajapakse CS, Magland JF, Wald MJ, et al. Computational biomechanics of the distal tibia from high-resolution MR and micro-CT images. Bone 2010;47(3):556–563.

21. Wehrli FW, Rajapakse CS, Magland JF, Snyder PJ. Mechanical implications of estrogen supplementation in early postmenopausal women. J Bone Miner Res 2010;25(6):1406–1414.

22. Zhang XH, Liu XS, Vasilic B, et al. In vivo microMRI-based finite element and morphological analyses of tibial trabecular bone in eugonadal and hypogonadal men before and after testosterone treatment. J Bone Miner Res 2008;23(9):1426–1434.

23. Almond MK, Kwan JT, Evans K, Cunningham J. Loss of regional bone mineral density in the first 12 months following renal transplantation. Nephron 1994;66(1):52–57.

24. Kodras K, Haas M. Effect of kidney transplantation on bone. Eur J Clin Invest 2006;36(Suppl 2):63–75.

25. Nickolas TL, Leonard MB, Shane E. Chronic kidney disease and bone fracture: a growing concern. Kidney Int 2008;74(6):721–731.

26. Julian BA, Laskow DA, Dubovsky J, Dubovsky EV, Curtis JJ, Quarles LD. Rapid loss of vertebral mineral density after renal transplantation. N Engl J Med 1991;325(8):544–550.

27. Patel S, Kwan JT, McCloskey E, et al. Prevalence and causes of low bone density and fractures in kidney transplant patients. J Bone Miner Res 2001;16(10):1863–1870.

28. Rajapakse CS, Magland JF, Wehrli FW. Fast prospective registration of in vivo MR images of trabecular bone microstructure in longitudinal studies. Magn Reson Med 2008;59(5):1120–1126.

29. Magland JF, Wald MJ, Wehrli FW. Spin-echo micro-MRI of trabecular bone using improved 3D fast large-angle spin-echo (FLASE). Magn Reson Med 2009;61(5):1114–1121.

30. Song HK, Wehrli FW. In vivo micro-imaging using alternating navigator echoes with applications to cancellous bone structural analysis. Magn Reson Med 1999;41(5):947–953.

31. Lin W, Ladinsky GA, Wehrli FW, Song HK. Image metric-based correction (autofocusing) of motion artifacts in high-resolution trabecular bone imaging. J Magn Reson Imaging 2007;26(1):191–197.

32. Bhagat YA, Rajapakse CS, Magland JF, et al. On the significance of motion degradation in high-resolution 3D µMRI of trabecular bone. Acad Radiol 2011;18(10):1205–1216.

33. Vasilic B, Wehrli FW. A novel local thresholding algorithm for trabecular bone volume fraction mapping in the limited spatial resolution regime of in vivo MRI. IEEE Trans Med Imaging 2005;24(12):1574–1585.

34. Magland JF, Jones CE, Leonard MB, Wehrli FW. Retrospective 3D registration of trabecular bone MR images for longitudinal studies. J Magn Reson Imaging 2009;29(1):118–126.

35. Rajapakse CS, Magland JF, Wald MJ, et al. Estimation of relative stiffness contributions of cortical and trabecular compartments by MRI-based finite element analysis [abstr]. J Bone Miner Res 2008;23(Suppl):S366.

36. Zysset PK, Guo XE, Hoffler CE, Moore KE, Goldstein SA. Elastic modulus and hardness of cortical and trabecular bone lamellae measured by nanoindentation in the human femur. J Biomech 1999;32(10):1005–1012.

37. Pistoia W, van Rietbergen B, Lochmüller EM, Lill CA, Eckstein F, Rüegsegger P. Estimation of distal radius failure load with micro-finite element analysis models based on three-dimensional peripheral quantitative computed tomography images. Bone 2002;30(6):842–848.

38. Niebur GL, Feldstein MJ, Yuen JC, Chen TJ, Keaveny TM. High-resolution finite element models with tissue strength asymmetry accurately predict failure of trabecular bone. J Biomech 2000;33(12):1575–1583.

39. van Rietbergen B, Pistoia W, Ulrich D, Huiskes R, Ruegsegger P. Prediction of trabecular bone failure parameters using a tissue failure criterion and mFE analysis. Comput Simul & Model in Med 2000;1:98–101. http://www.mate.tue.nl/mate/showabstract.php/913.

40. Saha PK, Wehrli FW. Measurement of trabecular bone thickness in the limited resolution regime of in vivo MRI by fuzzy distance transform. IEEE Trans Med Imaging 2004;23(1):53–62.

41. Aroldi A, Tarantino A, Montagnino G, Cesana B, Cocucci C, Ponticelli C. Effects of three immunosuppressive regimens on vertebral bone density in renal transplant recipients: a prospective study. Transplantation 1997;63(3):380–386.

42. Coco M, Glicklich D, Faugere MC, et al. Prevention of bone loss in renal transplant recipients: a prospective, randomized trial of intravenous pamidronate. J Am Soc Nephrol 2003;14(10):2669–2676.

43. Kwan JT, Almond MK, Evans K, Cunningham J. Changes in total body bone mineral content and regional bone mineral density in renal patients following renal transplantation. Miner Electrolyte Metab 1992;18(2-5):166–168.

44. McIntyre HD, Menzies B, Rigby R, Perry-Keene DA, Hawley CM, Hardie IR. Long-term bone loss after renal transplantation: comparison of immunosuppressive regimens. Clin Transplant 1995;9(1):20–24.

45. Mikuls TR, Julian BA, Bartolucci A, Saag KG. Bone mineral density changes within six months of renal transplantation. Transplantation 2003;75(1):49–54.

46. van den Ham EC, Kooman JP, Christiaans ML, van Hooff JP. The influence of early steroid withdrawal on body composition and bone mineral density in renal transplantation patients. Transpl Int 2003;16(2):82–87.

47. Grotz WH, Mundinger FA, Müller CB, et al. Trabecular bone architecture in female renal allograft recipients: assessed by computed tomography. Nephrol Dial Transplant 1997;12(3):564–569.

48. Cruz EA, Lugon JR, Jorgetti V, Draibe SA, Carvalho AB. Histologic evolution of bone disease 6 months after successful kidney transplantation. Am J Kidney Dis 2004;44(4):747–756.

49. Haas M, Leko-Mohr Z, Roschger P, et al. Zoledronic acid to prevent bone loss in the first 6 months after renal transplantation. Kidney Int 2003;63(3):1130–1136.

50. MacNeil JA, Boyd SK. Load distribution and the predictive power of morphological indices in the distal radius and tibia by high resolution peripheral quantitative computed tomography. Bone 2007;41(1):129–137.

51. Liu XS, Zhang XH, Rajapakse CS, et al. Accuracy of high-resolution in vivo micro magnetic resonance imaging for measurements of microstructural and mechanical properties of human distal tibial bone. J Bone Miner Res 2010;25(9):2039–2050.

52. Bevill G, Keaveny TM. Trabecular bone strength predictions using finite element analysis of micro-scale images at limited spatial resolution. Bone 2009;44(4):579–584.

53. Lam SC, Wald MJ, Rajapakse CS, Liu Y, Saha PK, Wehrli FW. Performance of the MRI-based virtual bone biopsy in the distal radius: serial reproducibility and reliability of structural and mechanical parameters in women representative of osteoporosis study populations. Bone 2011;49(4):895–903.

54. Wald MJ, Magland JF, Rajapakse CS, Wehrli FW. Structural and mechanical parameters of trabecular bone estimated from in vivo high-resolution magnetic resonance images at 3 tesla field strength. J Magn Reson Imaging 2010;31(5):1157–1168.

55. Krug R, Burghardt AJ, Majumdar S, Link TM. High-resolution imaging techniques for the assessment of osteoporosis. Radiol Clin North Am 2010;48(3):601–621.

56. Ladinsky GA, Vasilic B, Popescu AM, et al. Trabecular structure quantified with the MRI-based virtual bone biopsy in postmenopausal women contributes to vertebral deformity burden independent of areal vertebral BMD. J Bone Miner Res 2008;23(1):64–74.

57. Link TM, Bauer J, Kollstedt A, et al. Trabecular bone structure of the distal radius, the calcaneus, and the spine: which site predicts fracture status of the spine best? Invest Radiol 2004;39(8):487–497.

58. Lochmüller EM, Lill CA, Kuhn V, Schneider E, Eckstein F. Radius bone strength in bending, compression, and falling and its correlation with clinical densitometry at multiple sites. J Bone Miner Res 2002;17(9):1629–1638.